Remodeling of lipid landscape in high fat fed very-long chain acyl-CoA dehydrogenase null mice favors pro-arrhythmic polyunsaturated fatty acids and their downstream metabolites

Bruno Lefort, Roselle Gélinas, Anik Forest, Bertrand Bouchard, Caroline Daneault, Isabelle Robillard Frayne, Jérôme Roy, Camille Oger, Karine Greffard, Jean-Marie Galano, et al.

BBA - Molecular Basis of Disease 1869 (2023) 166843

Contents lists available at ScienceDirect

BBA - Molecular Basis of Disease

journal homepage: www.elsevier.com/locate/bbadis

Remodeling of lipid landscape in high fat fed very-long chain acyl-CoA dehydrogenase null mice favors pro-arrhythmic polyunsaturated fatty acids and their downstream metabolites

Bruno Lefort [a,b,c,1], Roselle Gélinas [a,d,1], Anik Forest [a], Bertrand Bouchard [a], Caroline Daneault [a], Isabelle Robillard Frayne [a], Jérôme Roy [e,f], Camille Oger [e], Karine Greffard [g], Jean-Marie Galano [e], Thierry Durand [e], François Labarthe [c], Jean-François Bilodeau [g,h], Matthieu Ruiz [a,i,*], Christine Des Rosiers [a,i,*]

[a] Montreal Heart Institute Research Centre, Montreal, Canada
[b] Institut des Cardiopathies Congénitales de Tours et FHU Precicare, CHU Tours, Tours, France
[c] INSERM UMR 1069 et Université François Rabelais, Tours, France
[d] Present address: CHU Ste-Justine Research Center, Montreal, Quebec, Canada
[e] Institut des Biomolécules Max Mousseron, Pôle Chimie Balard Recherche, UMR 5247, Université de Montpellier, CNRS, ENSCM, Montpellier, France
[f] INRAE, Université de Pau et des Pays de l'Adour, E2S UPPA, UMR1419 Nutrition Metabolism and Aquaculture, Aquapôle, F-64310 Saint-Pée-sur-Nivelle, France.
[g] Axe endocrinologie et néphrologie, CHU de Québec, Université Laval, Québec, Canada
[h] Department of Nutrition, Faculty of medicine, Université Laval, Quebec, Canada
[i] Department of Nutrition, Faculty of medicine, Université de Montréal, Montreal, Canada

ARTICLE INFO

Keywords:
VLCAD deficiency
Lipidomic
Prostane
Calcium homeostasis
Endoplasmic reticulum stress

ABSTRACT

Very-long chain acyl-CoA dehydrogenase (VLCAD) catalyzes the initial step of mitochondrial long chain (LC) fatty acid β-oxidation (FAO). Inherited VLCAD deficiency (VLCADD) predisposes to neonatal arrhythmias whose pathophysiology is still not understood. We hypothesized that VLCADD results in global disruption of cardiac complex lipid homeostasis, which may set conditions predisposing to arrhythmia. To test this, we assessed the cardiac lipidome and related molecular markers in seven-month-old VLCAD$^{-/-}$ mice, which mimic to some extent the human cardiac phenotype. Mice were sacrificed in the fed or fasted state after receiving for two weeks a chow or a high-fat diet (HFD), the latter condition being known to worsen symptoms in human VLCADD. Compared to their littermate counterparts, HFD/fasted VLCAD$^{-/-}$ mouse hearts displayed the following lipid alterations: (1) Lower LC, but higher VLC-acylcarnitines accumulation, (2) higher levels of arachidonic acid (AA) and lower docosahexaenoic acid (DHA) contents in glycerophospholipids (GPLs), as well as (3) corresponding changes in pro-arrhythmogenic AA-derived isoprostanes and thromboxane B_2 (higher), and anti-arrythmogenic DHA-derived neuroprostanes (lower). These changes were associated with remodeling in the expression of gene or protein markers of (1) GPLs remodeling: higher calcium-dependent phospholipase A2 and lysophosphatidylcholine-acyltransferase 2, (2) calcium handling perturbations, and (3) endoplasmic reticulum stress. Altogether, these results highlight global lipid dyshomeostasis beyond FAO in VLCAD$^{-/-}$ mouse hearts, which may set conditions predisposing the hearts to calcium mishandling and endoplasmic reticulum stress and thereby may contribute to the pathogenesis of arrhythmias in VLCADD in mice as well as in humans.

Abbreviations: AA, arachidonic acid; AC, acylcarnitine; AGPAT, 1-acylglycerol-3-phosphate O-acyltransferase; ARC, voltage independent AA-regulated calcium channel; CD, chow diet; DHA, docosahexaenoic acid; ER, endoplasmic reticulum; HFD, high fat diet; IsoP, isoprostane; LCFA, long chain fatty acid; LPC, lysophosphatidylcholine; LPCAT, lysophosphatidylcholine acyltransferase; LPE, lysophosphatidylethanolamine; MS, mass spectrometry; NeuroP, neuroprostane; PL, phospholipid; PLA2, phospholipase A2; PLB, phospholamban; PUFA, poly-unsaturated fatty acid; RyR2, ryanodine receptor 2; SERCA2a, sarco/endoplasmic reticulum Ca^{2+} ATPase; TXA_2, thromboxane A_2; TXB_2, thromboxane B_2; VLCAD, very long chain acylCoA dehydrogenase; VLCADD, VLCAD deficiency.

* Corresponding authors at: Montreal Heart Institute, Research Center, 5000 Bélanger Street East, room 5350, Montreal, Quebec H1T 1C8, Canada.
E-mail addresses: matthieu.ruiz@umontreal.ca (M. Ruiz), christine.des.rosiers@umontreal.ca (C. Des Rosiers).

[1] These authors contributed equally to this work.

https://doi.org/10.1016/j.bbadis.2023.166843
Received 6 February 2023; Received in revised form 20 July 2023; Accepted 4 August 2023
Available online 7 August 2023

1. Introduction

Very-long chain acyl-CoA dehydrogenase (VLCAD) catalyzes the first step of long-chain fatty acid (LCFA) mitochondrial β-oxidation. Inherited VLCAD deficiency (VLCADD) (OMIM #201475), the most prevalent mitochondrial LCFA oxidation disorder (~1:30000 births [1]), is associated with a broad range of clinical phenotypes. The most severe form of the disease occurs mostly in infants and is characterized by potentially lethal cardiac lesions including cardiomyopathy, pericardial effusion and/or arrhythmias [2–5]. Diagnosis of VLCADD relies on plasma accumulation of long-chain acylcarnitines (LC-ACs) and especially tetradecenoylcarnitine (C14:1) [6]. VLCAD deficiency is confirmed by assessing VLCAD enzyme activity and FA oxidation flux using labeled oleate or palmitate in patient fibroblasts or lymphocytes [7] and its gene mutation (*ACADVL*) is more commonly identified using Sanger methodology [8]. Even though the prognosis of VLCADD has substantially improved since its inclusion in newborn screening programs promoting early care in the detected children [9,10], a better understanding of the pathophysiology of VLCADD is warranted specially to identify new therapeutic strategies, as current ones failed to prevent clinical symptoms in patients with severe VLCADD [11,12].

Energy deficiency is commonly considered as the main cause of symptoms in patients with VLCADD. Additionally, lipid intermediates accumulating upstream of the defective enzyme in fibroblasts from patients with VLCADD, such as LC-ACs and LC-acyl-CoAs as well as complex lipids comprising ceramides or diacylglycerols [13], have been shown to have deleterious effects in various experimental models. These effects include endoplasmic reticulum (ER) stress response in C2C12 myotubes [14], inflammation through the activation of the JNK/ERK/p38 pathway in RAW 264.7 cells [15] as well as in adipocytes isolated from diabetic or obese patients [16], decreased mitochondrial energy production in fibroblasts derived from patients with LCFA oxidation defects [17], alteration of Krebs cycle enzymes activities in rat hearts [18] and dysregulation of ionic channels embedded in cellular membrane in HEK293 cells [19].

A mouse model of VLCADD ($VLCAD^{-/-}$) has been developed [20,21], albeit it does not reproduce exactly the pathogenesis of VLCADD in human. Such discrepancy has been attributed to the unexpected capacity of $VLCAD^{-/-}$ mice to oxidize LCFAs, likely due to compensatory mechanisms involving the enzyme long chain acyl-CoA dehydrogenase (LCAD), which is present in mice, while in humans, its expression is low in organs with high fatty acid β-oxidation (FAO) rates such as liver, muscle and heart [22,23]. In support of this notion, $LCAD^{-/-}$ mice present a more severe phenotype than their $VLCAD^{-/-}$ counterparts [24]. Nevertheless, $VLCAD^{-/-}$ mice mimic some of the human phenotype as they gradually develop cardiac dysfunction [25] and inducible ventricular tachycardia [21]. In addition, we have demonstrated that despite maintaining normal cardiac contractile function *ex vivo*, $VLCAD^{-/-}$ mice exhibit prolongation of the QT interval *in vivo*. Furthermore, these mice present unexpected cardiac lipid alterations, such as age- and condition-dependent reduced levels of docosahexaenoic acid (C22:6*n-3*, DHA) in glycerophospholipids (GPLs) [23]. The latter finding is of particular interest given the known association between *n-3* polyunsaturated fatty acids (PUFAs) and cardiac dysfunction, particularly arrhythmias and ventricular tachycardia [26–28]. The coverage of lipids beyond FAs, including various GPL subclasses or DHA related bioactive metabolites were, however, limited, as were the potential molecular mechanisms that could be involved in eliciting arrhythmias. Such bioactive lipids include F_4-neuroprostanes (F_4-NeuroP), which are derivative products of non-enzymatic oxidation of DHA that exert anti-arrhythmic properties in isolated ventricular cardiomyocytes and in post myocardial infarcted mice [29], and displayed cardio-protective properties by reducing apoptosis [30,31].

Hence, this study aimed at further characterizing complex lipid perturbations of $VLCAD^{-/-}$ mice using a combination of comprehensive untargeted and targeted lipidomic methods by liquid chromatography-mass spectrometry (LC-MS). Based on our previous findings of lower cardiac DHA content in GPLs in 7-month-old $VLCAD^{-/-}$ *vs.* control mice fed a high fat diet (HFD) *vs.* a standard chow diet (CD), we have used similarly aged mice and diets. Using mice under the CD/fed condition as baseline, we aimed at testing the impact of a condition known to worsen cardiac symptoms in human with VLCADD, namely FA overload as it occurs under a high-fat diet and fasting (HFD/fasted), where energy metabolism depends predominantly on FAO. Our findings show that under the latter condition, $VLCAD^{-/-}$ mice have exacerbated changes in heart tissue PUFA C22:6*n-3* (DHA; lower) *vs* C20:4*n-6* (arachidonic acid; AA; higher) content in GPLs. and in their respective downstream biologically active metabolites, F_4-NeuroP (lower) and F_2-isoprostanes (F_2-IsoP; higher). Since the latter changes suggested a tipping of the balance towards pro-arrhythmic metabolites, we then also aimed at evaluating alterations in molecular markers reflecting potential mechanisms linked to perturbations in calcium homeostasis as well as the endoplasmic reticulum stress response.

2. Materials and methods

2.1. Animals and study design

2.1.1. Animals

Animal experiments were approved by the local animal care committee in agreement with the guidelines of the Canadian Council on Animal Care. $VLCAD^{-/-}$ mice (129svJ X C57BL/6 J genetic background) were kindly provided by Dr. Arnold Strauss (University of Cincinnati, College of Medicine [21]). $VLCAD^{-/-}$ males were crossed with C57Bl/6 J females to generate heterozygous $VLCAD^{+/-}$ mice. Mating of heterozygous mice then produced $VLCAD^{-/-}$ mice and control littermate counterparts ($VLCAD^{+/+}$). All animals were genotyped as previously described [23]. For this study, male mice were housed in a specific pathogen-free facility under a 12-h light/dark cycle at constant temperature and with access to water and food *ad libitum* until they reached 7-month of age. Thereafter, they were divided in different experimental groups.

2.1.2. Study design

Based on our previous findings demonstrating lowest cardiac DHA levels in 7-month-old VLCAD-/- *vs.* VLCAD mice after 2-week of high fat feeding [23], this study was designed to assess broad changes in the cardiac lipidome of these mice under baseline condition and under a condition mimicking metabolic decompensation in human VLCADD, namely FA overload as it occurs under fasting and with a HFD. Therefore, 7-month-old $VLCAD^{-/-}$ and $VLCAD^{+/+}$ mice were each divided into two groups, which were fed for 2 weeks either a chow diet (CD; Harlan Teklad no. 2018; 3.1 kcal/g) or a high-fat diet (HFD; Harlan Teklad no. 03584; 5.4 kcal/g) *ad libitum*. The percent calories from carbohydrates, lipids and proteins from these diets was 58/18/24 and 26.6/58.4/15, respectively and their FA composition is provided in Supplementary Table 1. All mice were then sacrificed under anesthesia using ketamine (100 mg/mL) and xylazine (20 mg/mL) either in fed state for the CD group (CD/fed; reflecting baseline or control condition) or after fasting for 24 h for the HFD group (HFD/fasted; reflecting the metabolic decompensation condition under FA overload). Hearts were excised and immediately (within 2–3 s) snap-frozen with metal tongs chilled in liquid nitrogen and then stored at −80 °C.

2.2. Lipidomic analyses by HPLC-MS

2.2.1. Targeted analysis: Acylcarnitine (AC) profile

The semi-quantitative analysis of 54 ACs ware performed as previously described with slight modifications [32]. Briefly, ACs were extracted from pulverized heart under liquid nitrogen (~20 mg) using acetonitrile and ether after spiking with the following labeled internal standards: [$^2H_9$] free carnitine, [$^2H_3$] acetyl-carnitine, [$^2H_3$] propionyl-

carnitine, [$^2H_3$] butyryl-carnitine, [$^2H_3$] octanoyl-carnitine, [$^2H_3$] dodecanoyl-carnitine and [U-$^{13}C_4$] palmitoyl-carnitine. Supernatants were evaporated to dryness under a stream of nitrogen gas and dissolved in 50 μL methanol plus 50 μL water. Then 4 μL were injected onto a high performance liquid chromatography (HPLC; Atlantis dC18 silica column, 50 mm × 4.6 mm, particle size 3 μM, Waters) coupled to a 6460 Triple Quadrupole (QQQ) equipped with an electrospray ionization Jet Stream source (Agilent Technologies). Chromatographic separation was achieved as previously described [32]. Data were acquired in positive dynamic MRM mode for parent ions of *m/z* 85 and 60 and processed using Mass Hunter QQQ quantitative software (version B.07, Agilent technologies). Semi-quantitative analysis was performed for each AC by normalization to the selected internal standard (the closest in terms of chain length).

2.2.2. Targeted analysis: Quantification of F_4-NeuroP, F_2-IsoP and TXB_2

F_4-NeuroP, F_2-IsoP and TXB_2 quantification were performed as previously described with modifications [33]. Briefly, pulverized hearts under liquid nitrogen were supplemented with butylated hydroxytoluene plus indomethacin and spiked with the following internal standards:10-F_{4t}-NeuroP-d4, 10-*epi*-10-F_{4t}-NeuroP-d4, 5-F_{2t}-IsoP-d11, 8-F_{2t}-IsoP-d4, 15-F_{2t}-IsoP-d4 and TBX_2-d4. Then, an alkaline solution was added before sample processing in solid phase extraction cartridges (Strata-X, 60 mg/3 cc, Phenomenex, Torrance, CA, USA) beforehand preconditioned with methanol and 50 mM sodium acetate buffer (pH 3). Cartridges were then washed twice: first with water and second with hexane:ethyl acetate (75:25 *v*/v). Elution was done with 3 mL of methyl formate. Eluate was concentrated until dryness under a stream of nitrogen and reconstituted with 60 μL of a solution containing 13.5 % acetonitrile, 31.5 % methanol and 0.01 % acetic acid in water. LC-MS/MS analysis was carried out as previously described [34] with modifications. The latter included column temperature set at 45 °C and chromatographic separation which was achieved using a gradient of 3 solvents (A: 0.01 % acetic acid in water (v/v); and B: 0.01 % acetic acid in acetonitrile (v/v) and C: 0.01 % acetic acid in methanol) as followed: First, solvent A was ramped from 55 % to 8.2 % and solvent B from 0 % to 36.7 % over 13.2 min. Second, a linear gradient (0.1 min) to 80 % (B) and 15 % (C) respectively was applied and maintained for 2.2 min. Then solvent A was decreased to 0 % and B to 45 % in 0.1 min and maintained for an additional 5 min to complete the 20.6 min run. Analyses were analyzed using the multiple-reaction monitoring (MRM) mode. Acquisition was done using Analyst 1.6.2 and quantification was performed using MultiQuant 3.0.2 software (AB Sciex).

2.2.3. Untargeted analysis: comprehensive lipidomic analysis

Untargeted lipidomic analyses were conducted using a previously validated workflow [35]. Briefly, total lipids were extracted from 40 mg of pulverized hearts under liquid nitrogen using in methyl *tert*-butyl ether (MTBE) and ethyl acetate after spiking with the following internal standards lysophosphatidylcholine (LPC) 13:0, phosphatidylcholine (PC) 19:0/19:0, PC14:0/14:0, phosphatidylserine (PS) 12:0/12:0, phosphatidylglycerol (PG) 15:0/15:0 and phosphatidylethanolamine (PE) 17:0/17:0). Supernatants were evaporated using a Speed Vacuum concentrator overnight, dissolved in methanol/chloroform (2,1) and aliquots (50 μL) were stored at −80 °C until use. LC-MS analysis were performed by injection of 1 μL onto a 1290 Infinity HPLC (Zorbax Eclipse plus C18 column, 2.1 mm × 100 mm, particle size 1.8 μm, Agilent Technologies) coupled to a 6530 accurate mass Quantitative Time of Flight (QTOF) MS system equipped with a dual electrospray (ESI) source and operated in the positive ionization mode (Agilent Technologies Inc.). Lipid were eluted over 83 min at constant temperature of 40 °C using a gradient of solvent A (0.2 % formic acid and 10 mM ammonium formate in water) and B (0.2 % formic acid and 5 mM ammonium formate in methanol:acetonitrile:MTBE, 55:35:10 [v/v/v]).

The raw lipidomic dataset has been deposited at Metabolomics Workbench (www.metabolomicsworkbench.org). The study reference number is # ST002569 and the link is: https://doi.org/10.21228/M8ND9B. MS raw data processing was achieved using the Mass Hunter Qualitative Analysis software package (version B.07) for peak picking and a bioinformatic script (available at MetaboICM/Metaborose (github.com) and MetaboICM/Data-processing: Script (github.com)), which we have developed and encoded in both Perl and R languages to enable optimal MS data alignment, retention time (RT) correction, filtering of presence, normalization, batch effect correction, and missing data imputation. The resulting final dataset lists reproducible high quality MS signals referred as features, which are characterized by a mass-over-charge (*m/z*), a corrected signal intensity, and a RT. Lipid annotation was achieved on features that passed our subjective selected criteria of significance (a corrected *p*-value of 0.05 following Benjamini-Hochberg correction; corresponding to a *p* value of 0.0038; and a fold-change (FC) < 0.67 or > 1.5) for the comparison of VLCAD$^{-/-}$ *vs* VLCAD$^{+/+}$ mice receiving the same diet. Selected features were annotated by alignment with our in-house database containing >500 previously annotated lipids using MS/MS and public databases (Metlin and Lipid Map), as well as by MS/MS analyses, from which mass spectra were manually interpreted to identify the polar head and acyl chains based on their fragmentation pattern, as previously described in detail [35].

2.3. Molecular analyses

2.3.1. Real time qPCR analysis

Total RNA was isolated from pulverizing frozen heart using the RNeasy mini kit (Qiagen, Hilden, Germany). Reverse transcription of total RNA was performed with the high-capacity cDNA reverse transcription kit (Applied Biosystems, Burlington, ON, Canada) according to the manufacturer recommendations. Gene transcript levels of the following genes were assessed: acylglycerol-3-phosphate O-acyltransferases 1, 2 and 3 (Agpat1, Agpat2, Agpat3), LPC acyltransferase 2 and 3 (Lpcat2, Lpcat3), phospholipase A2 group 4 and group 6 (Pla2G4a, Pla2G6), fatty acid delta 5 and delta 6 desaturase (Fads1, Fads2), fatty acid elongase 5 (Elovl5), acyl-CoA oxidase 1 (ACOX1), peroxisomal-3-oxoacyl-CoA thiolase (PTHIO/Acaa1), peroxisomal bifunctional enzyme (PBE/Ehhadh), multifunctional protein 2 (Mfp2), CHOP (Ddit3), TATA box binding protein (TBP). The list and sequences of primers used are reported in Supplementary Table 2. RT qPCR were conducted as previously described [36]. Gene transcript levels were normalized to the level of TBP transcript expression.

2.3.2. Western Blot analysis

Protein homogenates from pulverizing heart were separated on SDS polyacrylamide gel then transferred to nitrocellulose as previously described [36]. Detection was carried out using primary antibodies against GRP78/BIP (Abcam, 1:1,000), CHOP (Cell Signaling Technology, 1:1,000), Ryanodine receptor 2 (RyR2) (Abcam, 1:2,000), phospholamban (PLB) (EMD Millipore, 1:1,000), SERCA2a (Thermo Scientific, 1:1,000). The HRP-conjugated β-Actin antibody (Santa Cruz Biotechnology) served as loading control. Signal were detected with the ChemiDoc Imaging System (Bio-Rad Laboratories, Berkeley, USA), and quantified with the Image Lab 6.0 software (Bio-Rad Laboratories, Berkeley, USA).

2.4. Statistical analysis

For untargeted lipidomic analysis, the final corrected dataset containing all features for VLCAD$^{+/+}$ and VLCAD$^{-/-}$ mice under both dietary condition was imported into Mass Professional Pro (MPP: version B.14.00; Agilent Technologies Inc.) for statistical analysis. Independent testing of each feature was achieved on log 2 transformed data using an unpaired Student *t*-test with Benjamini-Hochberg correction for comparison of VLCAD$^{+/+}$ *vs* VLCAD$^{-/-}$ mice for each dietary condition. The selected threshold of significance was a corrected *p*-value <0.05 as an

estimation of false discovery rate of 5 % and an absolute fold change of 1.5. Data for ACs, F_2-IsoP and F_4-NeuroP, as well as protein and gene expression were compared between VLCAD$^{+/+}$ and VLCAD$^{-/-}$ mice under each dietary condition separately using an unpaired Student t-test or the non-parametric Mann and Whitney test whenever variances were significantly unequal using GraphPad Prism version 9.0 (GraphPad software, Inc.) and significance threshold was set as $p < 0.05$. Supplementary analyses of these data were also conducted using a 2-way Anova (genotype *vs.* condition) and post-hoc Fisher's LSD test. Data are depicted as volcano plots as well as a heat map whereby the median of scaled lipids for each group was plotted using "pheatmap" in R (untargeted lipidomics) and as dotted box plots, where the midline represents the median, the box represents the interquartile range (IQR) between the first and third quartile, and dots are individual values.

3. Results

3.1. Targeted cardiac acylcarnitine (AC) profiling reveals accumulation in very-long, albeit lower long-chain, ACs in VLCAD$^{-/-}$ mouse hearts

VLCADD is characterized by high plasma levels of LC-ACs, C14-ACs in humans [37,38] and C16- and C18-ACs in VLCAD$^{-/-}$ mice [20]. In contrast, lower cardiac LC-ACs was reported in VLCAD$^{-/-}$ mice [39], albeit the impact of high fat feeding had not been examined. We therefore first assessed whether ACs were affected in heart tissues of VLCAD$^{-/-}$ mice under our two dietary conditions using targeted profiling by LC-QQQ. Results showed that compared to their VLCAD$^{+/+}$ littermate counterparts fed the same diet and sacrificed under the same fasting or feeding condition, CD/fed VLCAD$^{-/-}$ mice exhibited higher cardiac levels of VLC-AC 24:0 (5-fold, $p < 0.01$); while the majority of other ACs, LC-AC, medium chain (MC)- and short chain (SC)-AC were significantly lower (up to 8.5-fold, $p < 0.001$) (Fig. 1A). Under the HFD/fasted condition, additional VLC-AC species were also significantly higher in VLCAD$^{-/-}$ mice, namely with 20 to 24 carbons (up to 6-fold, $p < 0.05$) while changes in the level of other ACs were essentially similar to those observed for the CD condition (Fig. 1B). The complete list of measured ACs is provided in Supplementary Table 4. Altogether, our findings of lower LC-ACs combined with accumulation of VLC-ACs suggest perturbations in FA metabolism that go beyond mitochondrial FAO, which may involve their elongation/desaturation or the peroxisomes. They also do not support a role for LC-ACs accumulating intracellularly as a potential mechanism underlying the cardiac phenotype in VLCAD$^{-/-}$ mice.

Acylcarnitine profiling ($n = 8$ per condition) was performed by LC-QQQ on pulverized snap-frozen heart tissue of VLCAD$^{-/-}$ and VLCAD$^{+/+}$ mice in A) CD/fed condition and B) high fat diet (HFD)/fasted condition. Results are expressed as fold-changes in VLCAD$^{-/-}$ *vs* VLCAD$^{+/+}$ mice and presented as dotted box plots where the midline represents the median, the box represents the interquartile range (IQR) between the first and third quartile, and dots are individual values. Statistics: $*p < 0.05$, $**p < 0.01$, $***p < 0.001$ using unpaired Student *t*-test. Statistical results are also supported by supplementary analysis using a 2-way Anova and post-hoc Fisher's LSD test (Supplementary Tables 3A and 4).

3.2. Untargeted lipidomics unveils glycerophospholipid (GPL) acyl chain remodeling in VLCAD$^{-/-}$ mouse hearts that is exacerbated under the high fat diet (HFD)/fasted condition

Considering our previous finding of a lower DHA levels in GPLs in 7-month-old VLCAD$^{-/-}$ mice [23], the impact of VLCADD on cardiac complex lipids, particularly GPL sub-classes, was further characterized under CD/fed (baseline) and HFD/fasted (mimicking metabolic decompensation) conditions. For this, we used a previously validated high-resolution LC-QTOF-based untargeted lipidomic workflow optimized for isomer resolution, which can detect >1000 reproducible MS features (defined by a mass-to-charge ratio (*m/z*), retention time and signal intensity) covering 20 lipid sub-classes, including their acyl side chains [35].

The final dataset retained 2075 MS features eluting in the first 40 min of the chromatogram; this excluded glycerolipids because their MS signals were saturated under the HFD/fasted conditions. Using an unpaired *t*-test with Benjamini-Hochberg correction and applying a subjective threshold of corrected *p*-value<0.05 (corresponding to an uncorrected p-value <0.0038) and a fold-change (FC) > 1.5 or < 0.67, 93 and 189 MS features discriminated hearts from VLCAD$^{-/-}$ mice *vs* their littermate counterparts under the CD/fed (Fig. 2A) and HFD/fasted (Fig. 2B) condition (listed in Supplementary Tables 5 and 6). Twenty-nine and 47 unique lipids were annotated by MS/MS, shown as different colors in Fig. 2A-B, respectively, and also as a heatmap (Fig. S1 and Supplementary Table 7). While most lipids showed changes in the same direction in hearts from VLCAD$^{-/-}$ *vs.* control mice under both conditions, changes were of greater magnitude in the HFD/fasted condition. Hence, a higher proportion of lipids reached significance (47 *vs.* 29) under the HFD/fasted condition, of which 8 were common to both conditions. These lipids include LC-AC species such as C14:1-AC, which was lower in VLCAD$^{-/-}$ *vs* control mice under both conditions, concurring with the results of our targeted AC profiling; VLC-AC were,

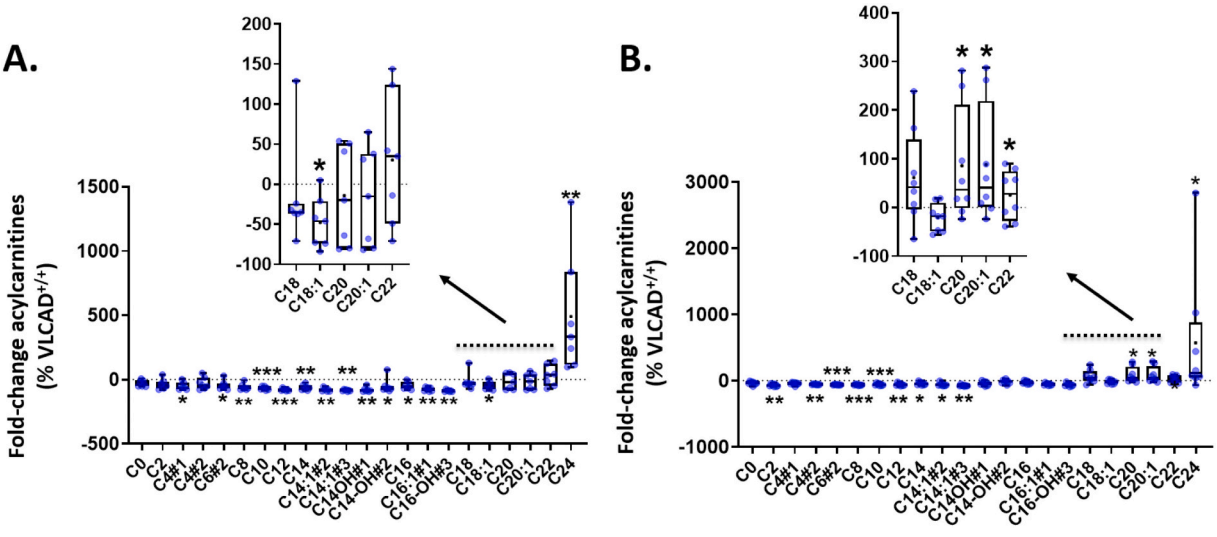

Fig. 1. Cardiac acylcarnitine (AC) profile alterations in VLCAD$^{-/-}$ mice under (A) chow fed (CD)/fed and (B) high fat diet (HFD)/fasted condition.

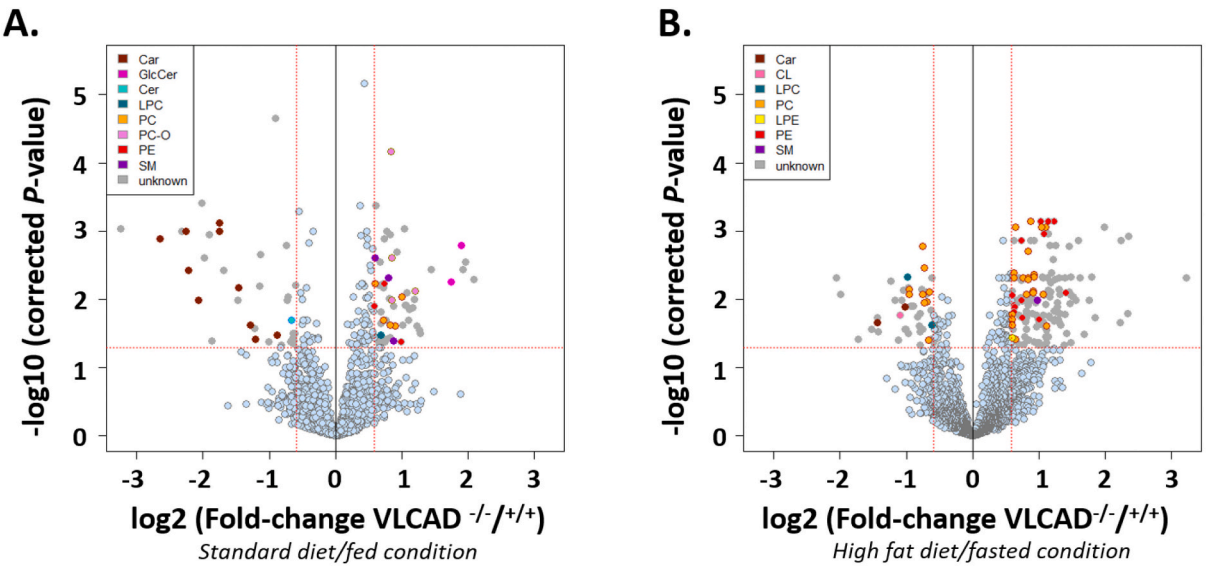

		Lipid sub-class											Total
		Car	Car(OH)	LPC	LPE	PC	PCO-	PE	SM	SM(OH)	Cer	Glc-Cer	CL	
# Unique lipids	STD -/- vs STD +/+ - FDR<0.05 & FC>1.5	7	3	1		5	4	3	2	1	1	2		29
	HF -/- vs HF +/+ - FDR<0.05 & FC>1.5	2		2	1	29		11	1				1	47

Fig. 2. Cardiac lipidome dyshomeostasis in VLCAD$^{-/-}$ mice under (A) CD/fed and (B) HFD/fasted condition.

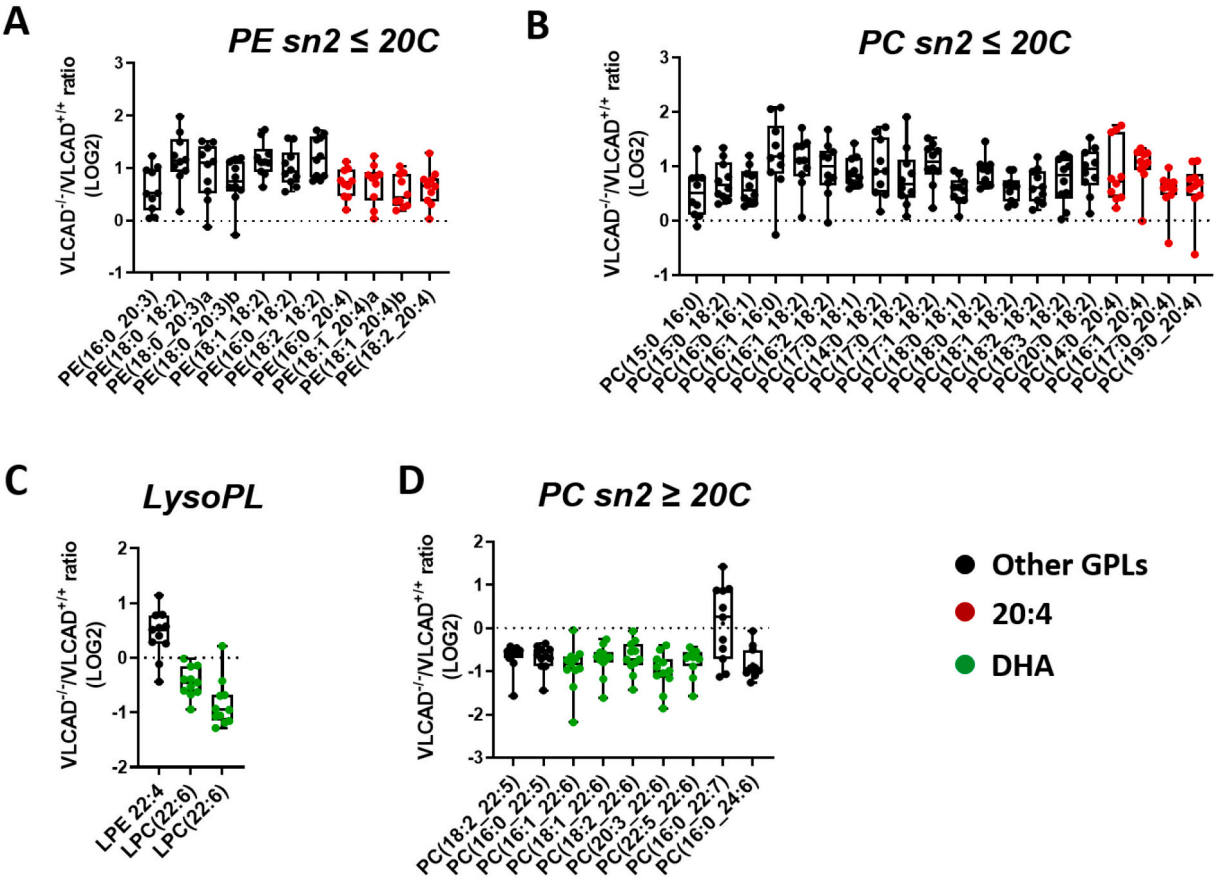

Fig. 3. Cardiac glycerophospholipid (GPL) acyl chain remodeling in VLCAD$^{-/-}$ mice under the HFD/fasted condition.

however, not detected using the untargeted lipidomic workflow, attributed to the sensitivity performance between the two methods. Other lipid (sub-) classes include sphingolipids (SPs), but predominantly GPLs, both phosphatidylcholine (PC) and phosphatidylethanolamine (PE) species.

Volcano plot showing the 2075 MS features retained in the final dataset following untargeted lipidomic analysis using high performance LC-QTOF of heart tissue samples of VLCAD$^{-/-}$ ($n = 11$ per condition) and VLCAD$^{+/+}$ ($n = 9$ per condition) mice under A) standard diet (CD)/fed and B) high fat diet (HFD)/fasted conditions. Data processing included all MS features eluting within 40 min; this excluded glycerolipids whose MS signals were saturated in the HFD/fasted condition. X-axes show fold-change (FC) ($\log_2$) in MS signal intensity values and y-axes the corresponding corrected *p*-values ($-\log_{10}$) for the comparison VLCAD$^{-/-}$ *vs* VLCAD$^{+/+}$ using an unpaired *t*-test with Benjamini-Hochberg correction. All 93 and 189 MS features discriminating VLCAD$^{-/-}$ *vs* VLCAD+/+ mice under the CD/fed A) and HFD/fasted B) condition, respectively (Listed in Supplementary Table 5 and 6) that passed the selected significance threshold of corrected p-value<0.05 (corresponding to an uncorrected p-value <0.0038; horizontal red line) and a fold-change (FC) > 1.5 or <0.67 (vertical dotted red lines) were analyses by MS/MS, of which 29 and 47 were annotated to unique lipids, respectively. Colors indicate lipid sub-classes. Car: acylcarnitine; Cer: Ceramide; CL: cardiolipin; LPC: lyso-phosphatidylcholine; LPE: lyso-phosphatidylethanolamine, PC: glycerophosphatidylcholine; PC-O: PC ether; PE: glycerophosphatidylethanolamine; SM: sphingomyelin.

Among GPLs, there was a greater number of species that was altered in VLCAD$^{-/-}$ *vs* controls in the HFD/fasted *vs* CD/fed condition (43 *vs* 13 GPLs, respectively) (Fig. 2 and S1; and Supplementary Table 7). Among the 43 annotated GPLs that discriminated VLCAD$^{-/-}$ *vs* control mouse hearts under the HFD/fasted condition (Fig. 3A-C), 32 were higher in VLCAD$^{-/-}$ mice, 31 of which contained an acyl chain with ≤20 carbons, 11 PEs (Fig. 3A) and 20 PCs (Fig. 3B), 8 of which were C20:4. In contrast, 11 GPLs were lower in VLCAD$^{-/-}$ mice and contained an acyl chain with ≥20 carbons, 9 PCs and 2 lysoPCs, 7 of which contained C22:6. (Fig. 3C, D). Although we are unable to confirm the position of double bonds in both C20:4 and C22:6, due to the lack of available commercial standards, based on our previous finding of similarly lower DHA, but higher AA content in cardiac GPL of 7-month-old VLCAD$^{-/-}$ mice fed a HFD assessed through quantitative targeted analysis [23], the GPL remodeling are likely to involve opposite changes in PUFA *n-6* AA (up) *vs n-3* DHA (down) in VLCAD$^{-/-}$ mice under the HFD/fasted condition, which is known to worsen cardiac symptoms in human VLCADD. Given the broader and greater changes in cardiac lipids in VLCAD−/− *vs.* VLCAD+/+ mice under the HFD/fasting condition than CD/fed, the former condition was the main focus of all subsequent metabolite and gene expression analyses.

Dotted box plots for the 43 GPLs discriminating VLCAD$^{-/-}$ from VLCAD$^{+/+}$ mouse hearts under the HFD/fasted condition using our selected significance threshold (corrected *p*-value<0.05; corresponding to an uncorrected p-value <0.0038; and fold-change (FC) > 1.5 or < 0.67) and that were annotated by MS/MS using LC-QTOF. Each dot represents a log2-transformed fold-change of MS intensity ratios for VLCAD$^{-/-}$ *vs* VLCAD+/+ mice ($n = 9$) for the indicated GPL sub-class containing specific acyl side chain in *sn2* position: A) PE and B) PC with acyl chain with ≤20C; C) LysoPC and lyso PE; and D) PC with acyl chain with ≥20C. Red and green dots indicate GPLs containing arachidonic acid (AA; C20:4*n-6*) and docosahexaenoic acid (DHA; C22:6*n-3*), respectively; while all other GPLs are shown as black dots. PE: phosphatidylethanolamine, LPE: lysophosphatidylethanolamine, PC: phosphatidyl-choline, LPC: lysophosphatidylcholine, lysoPL: lysophospholipid, GPL: glycerophospholipid, DHA: docosahexaenoic acid.

3.3. VLCAD$^{-/-}$ mice show opposite changes in cardiac levels of biologically active DHA and AA downstream metabolites in the HFD/fasted condition

Further to our finding of a greater remodeling in cardiac GPLs containing PUFAs, especially C22:6 (lower) and C20:4 (higher), in VLCAD$^{-/-}$ mice under the HFD/fasted condition, we aimed at assessing the levels of C20:4*n-6* or arachidonic acid (AA)- and C22:6*n-3* or DHA-derived metabolites involved in relevant cardiac biological functions only in this specific condition. Specifically, our focus was on their non-enzymatic oxygenated metabolites F2-isoprostanes (F_2-IsoP) (from AA) and F_4-Neuroprostanes (F_4-NeuroP) (from DHA) [40]. Compared to their control counterparts, VLCAD$^{-/-}$ mouse hearts showed significantly higher levels of many of AA-derived metabolites F_2-IsoP (8-F_{2t}-IsoP: +31 %, $p < 0.05$; 5-F_{2c}-IsoP: +48 %, p < 0.05; and 5-*epi*-5-F_{2t}-IsoP: +39 %, p < 0.05; Fig. 4A) as well as thromboxane B_2 (TXB_2: +62 %, $p < 0.01$; Fig. 4B), a stable, biologically inactive metabolite of thromboxane A_2 (TXA_2) and endogenous mediator of inflammation generated from AA [41]. In contrast, VLCAD$^{-/-}$ mouse hearts had significantly lower levels for many of the DHA-derived metabolites F_4-NeuroP (10-F_{4t}-NeuroP: −20 %, p < 0.05; 20-F_{4t}-NeuroP: −51 %, $p < 0.001$; Fig. 4C). Altogether, these findings highlight a marked imbalance in the cardiac levels of AA- and DHA-derived non-enzymatic oxygenated metabolites in VLCAD$^{-/-}$ mice under the HFD/fasted condition.

Dotted box plots of concentrations of AA-derived non-enzymatic oxygenated F2-isoprostanes A) and thromboxane B2 B) as well as DHA-derived non-enzymatic oxygenated F4-neuroprostanes C) assessed by LC-MS in VLCAD$^{-/-}$ ($n = 8$) and VLCAD$^{+/+}$ ($n = 7$) mouse hearts under HFD/fasted condition. Statistics: *p < 0.05, **p < 0.01, ***p < 0.001 using an unpaired Student *t*-test. TBX_2: thromboxane B2, PG: prostaglandins.

3.4. VLCAD$^{-/-}$ mouse hearts show higher gene expression of calcium-dependent enzymes involved in GLP acyl chain remodeling

Further to our finding of a greater remodeling of cardiac GPL acyl chains in VLCAD$^{-/-}$ mouse hearts under the HFD/fasted condition, we assessed if this may be linked to changes in gene expression by measuring the expression of selected and relevant metabolic genes in VLCAD$^{-/-}$ and VLCAD$^{+/+}$ mice under this specific condition. These include genes encoding for enzymes involved in: i) GPL synthesis and FA remodeling, namely isoforms of lysophosphatidylcholine acyltransferase (LPCAT; *Lpcat2* and *Lpcat3*) and phospholipase A2 (PLA2; *Pla2g4* and *Pla2g6*) [42] as well as of 1-acylglycerol-3-phosphate O-acyltransferase (AGPAT; *Agapt1*, *Agapt2* and *Agapt3*) [43] (Fig. 5A-C); ii) PUFA (AA and DHA) synthesis through elongation and desaturation (*Elovl5*, *Fads1, Fads2*; Fig. 5D) or AA conversion to biologically active derivatives (*Alox5*, *Alox12*, *Alox15*; Fig. 5E), and iii) peroxisomal FA metabolism (*Acox1*; *Mfp2*; *Ehhadh*; *Pthio*; Fig. 5F). Interestingly, transcript levels for calcium-dependent (Fig. 5A), but not calcium-independent (Fig. 5B), enzyme isoforms, namely LPCAT2 (*Lpcat2)* and PLA2 group 4 (*Pla2g4*) were significantly higher in HFD/fasted VLCAD$^{-/-}$ *vs* VLCAD$^{+/+}$ mouse hearts (+89 %, $p < 0.05$ and + 63 %, p < 0.05). Transcript levels for all other above-mentioned metabolic genes were unchanged except that of *Alox 12*, which was significantly lower in VLCAD$^{-/-}$ *vs* VLCAD$^{+/+}$ mice (−42 %; Fig. 5E). Supplementary analysis showed that changes in gene expression for the aforementioned enzymes were similar under the CD/fed condition for the two groups of mice, except for *Fads1* and *Fads2,* which showed significantly higher transcript levels in VLCAD$^{-/-}$ hearts (+52 %; $p < 0.01$ and + 79 ± 17 %; p < 0.01 respectively, suggesting a possible adaptive change in this condition (Fig. S2; and Supplementary Table 3B for 2-Way Anova analysis results).

Dotted box plots of transcript levels assessed by RT-qPCR for genes encoding enzymes involved in: A-C) *GPL acyl chain remodeling*: Isoforms of A-B) lysophosphatidylcholine acyltransferase (LPCAT) and phospholipase A2 that are A) calcium-dependent (*LPCAT2; PLA2G4*) or B)

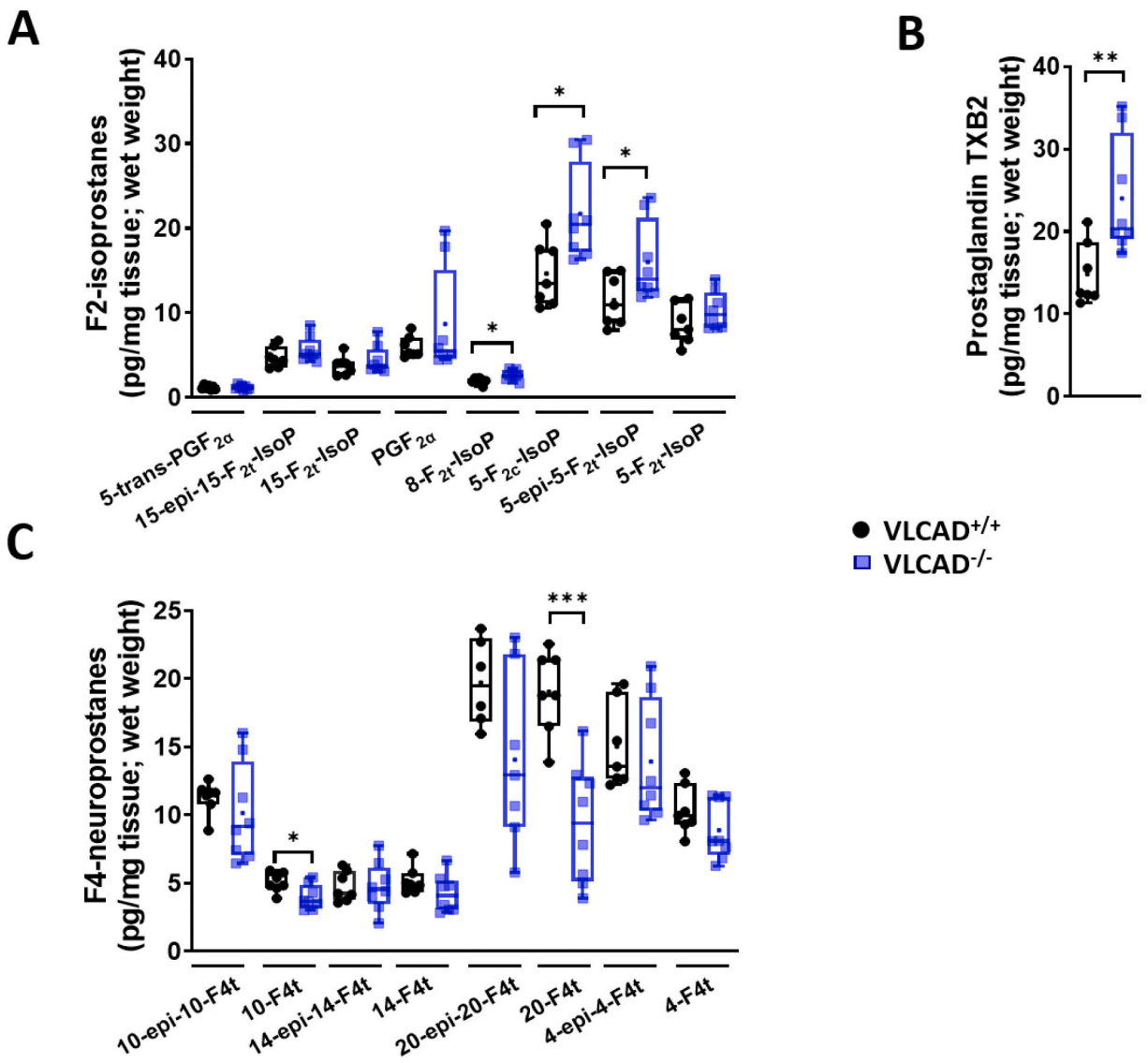

Fig. 4. Opposite changes in cardiac levels of AA- *vs* DHA-derived non-enzymatic oxygenated metabolites in VLCAD$^{-/-}$ mice under the HFD/fasted condition.

calcium-independent (*LPCAT3; PLA2G6*), as well as C) 1-acylglycerol-3-phosphate O-acyltransferase (*AGPAT1*; *AGPAT2*; *AGPAT3*); D) Synthesis of polyunsaturated fatty acids AA and DHA (*Elovl5*, *Fads1, Fads2*); E) AA conversion to biologically active derivatives (*Alox5*, *Alox12*, *Alox15*) and F) peroxisomal fatty acid metabolism (*Acox1*; *Mfp2*; *Ehhadh*; *Pthio*; Fig. 4F). Transcript levels for VLCAD$^{-/-}$ ($n = 7$) and VLCAD$^{+/+}$ mouse hearts ($n = 6$) under the HFD/fasted condition were normalized to TATA box binding protein (TBP) gene expression. Statistics: *$p < 0.05$, **$p <$ 0.001 using unpaired Student *t*-test.

Altogether, our finding of higher transcript levels of calcium-dependent, but not-calcium independent, enzymes involved in cardiac GPL remodeling in VLCAD$^{-/-}$ mouse hearts suggest calcium dyshomeostasis, which may contribute to GPL acyl chain remodeling in the absence of other adaptive changes.

3.5. VLCAD$^{-/-}$ mice show alterations in the expression of cardiac proteins involved in calcium homeostasis in the HFD/fasted condition

Given that our gene expression findings suggested alterations in calcium homeostasis, a process involved in ventricular arrhythmias [44], we assessed the cardiac expression of major endoplasmic reticulum (ER) proteins involved calcium homeostasis, namely sarco/endoplasmic reticulum Ca^{2+} ATPase (SERCA2a), phospholamban (PLB), and ryanodine receptor 2 (RyR2). We found significant differences in the cardiac levels of these proteins between HFD/fasted VLCAD$^{-/-}$ *vs* VLCAD$^{+/+}$ mice: specifically, levels for SERCA2a and PLB were higher (+35 %, $p < 0.05$ and + 95 %, $p < 0.001$, respectively; Fig. 6A, B), while that for RyR2 was lower (−55 %, $p < 0.01$, Fig. 6C). We, however, did not observe any significant changes in their phosphorylation on Ser16 for PLB and Ser2802 for RyR2 while the phosphorylated-to-total protein ratio appeared decreased for PLB (−66 %) but increased for RyR2 (+75 %). These differences between VLCAD$^{-/-}$ *vs* VLCAD$^{+/+}$ mouse hearts were, however, not observed in the CD/fed condition (Fig. S3 and Supplementary Table 3 for 2-way Anova analysis results). Taken together, these results suggest an altered regulation of cardiac proteins involved in intracellular calcium homeostasis in VLCAD$^{-/-}$ mice under the HFD/fasted condition.

A-C) Representative images (left panel) and quantification (dotted box plots; data normalized to β-actin) of immunoreactivity of key cardiac proteins involved in calcium handling assessed in VLCAD$^{-/-}$ and VLCAD$^{+/+}$ mouse hearts under the HFD/fasted condition ($n = 4$/group): A) sarcoplasmic/endoplasmic reticulum Ca^{2+} ATPase (SERCA2a), B) phospholamban (PLB) and C) ryanodine receptor 2 (RyR2). Statistics: *$p < 0.05$, **$p < 0.01$, ***p < 0.001, using an unpaired Student *t*-test.

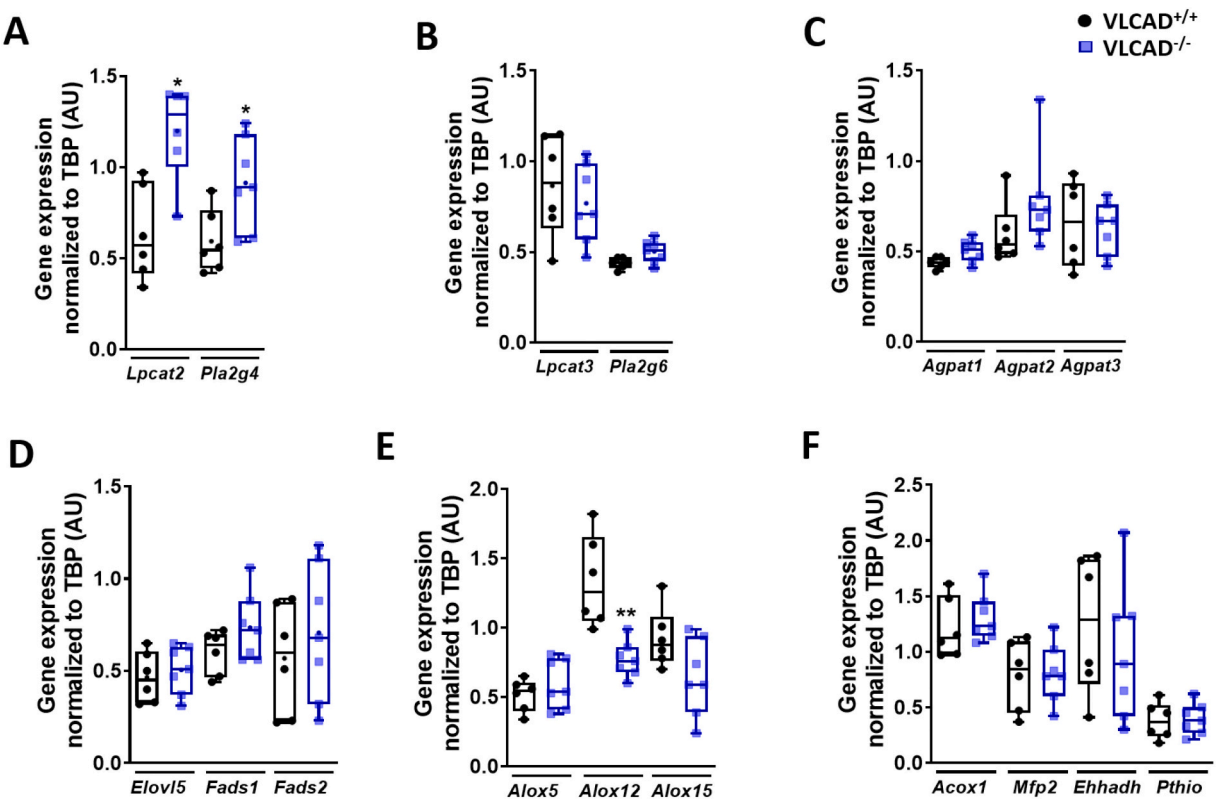

Fig. 5. Changes in cardiac gene expression of enzymes involved in GPL acyl chain remodeling and related metabolism in VLCAD$^{-/-}$ mice under the HFD/fasted condition.

3.6. VLCAD$^{-/-}$ mice show changes in cardiac protein and/or transcript levels of markers of endoplasmic reticulum (ER) stress in the HFD/fasted condition

Lastly, since GPL remodeling and calcium regulation occurs in the endoplasmic reticulum (ER) [45,46], and alterations in GPL fatty acyl content was reported to promote ER stress [47], a maladaptive response that may also contribute to arrhythmias [48,49], we assessed the cardiac expression of two recognized actors in this process, namely GRP78 (protein level) and CHOP (protein and transcript levels). It is noteworthy that neither gene nor protein expressions of GRP78 or CHOP differed between VLCAD$^{-/-}$ and VLCAD$^{+/+}$ mouse hearts in the CD/fed condition (Fig. S4 and Supplementary Table 3 for 2-way Anova analysis results). In contrast, cardiac GRP78 protein expression was significantly higher in VLCAD$^{-/-}$ *vs* VLCAD$^{+/+}$ mice in the HFD/fasted condition (+90 %, $p < 0.01$; Fig. 7A) as was CHOP transcript levels (+35 %, $p < 0.05$; Fig. 7B), although change in CHOP protein expression did not reach significance (+71 %, $p = 0.15$; Fig. 7A), Altogether these findings suggest that GPL remodeling in hearts from VLCAD$^{-/-}$ mice is associated ER stress under the HFD/fasted condition.

Representative images (top panel) and quantification of levels (dotted box plots; data normalized to β-actin) of immunoreactivity of key ER proteins, GRP78 and CHOP ($N = 4$ per group), and B) transcript levels of CHOP ($n = 7$ per group) normalized to TATA box binding protein (TBP) gene expression, in VLCAD$^{-/-}$ and VLCAD$^{+/+}$ mouse hearts under the HFD/fasted condition. Statistics: *p < 0.05, **p < 0.01 using an unpaired Student *t*-test.

4. Discussion

In this study, we applied MS-based targeted and untargeted lipidomics combined with molecular methods in a VLCAD$^{-/-}$ mouse model to identify perturbations in cardiac lipids beyond FAs as well as related molecular mechanisms potentially involved in reported cardiac rhythm manifestations in VLCADD. These analyses were conducted under two metabolic conditions, namely the CD/fed condition, representing the basal nutritional state, and the HFD/fasted condition, representing a condition of FA overload known to worsen the clinical phenotype in patients with VLCADD. Compared to their littermate counterparts, 7-month-old HFD/fasted VLCAD$^{-/-}$ mouse hearts displayed marked modifications of lipid composition including VLC-ACs accumulation, higher levels of AA and lower DHA contents in GPLs, concurring and expanding our previous findings [23], as well as corresponding changes in pro-arrhythmogenic AA-derived IsoP and TXB_2 and anti-arrythmogenic DHA-derived NeuroP. These changes were associated with remodeling in the expression of gene or protein markers of GPL remodeling, calcium handling perturbations and endoplasmic reticulum stress. Taken altogether our results highlights cardiac lipid perturbations under FA overload that may set conditions favouring the formation of pro-arrhythmic lipid PUFA metabolites.

Because LC-AC can affect negatively calcium homeostasis and mitochondrial function [14,17], we first conduced a targeted profiling of 78 ACs in VLCAD$^{-/-}$ mouse hearts. Concurring with previous report [39], cardiac LC-AC levels in VLCAD$^{-/-}$ mice were lower than controls, a finding that may be explained by the functional overlap between VLCAD and LCAD, the latter being active in mice rather than changes in mitochondrial FAO rates based on our previous findings of normal relative FAO flux when assessed in *ex vivo* working hearts from VLCAD$^{-/-}$ mice perfused with 0.4 to 1 mM ^{13}C-labeled palmitate under various basal and stress conditions [23]. One interesting finding of this study, however, is the higher cardiac level of VLC-ACs in VLCAD$^{-/-}$ mice, which is exacerbated in the HFD/fasted condition and may suggest increased shuttling of LCFA-CoAs towards elongation and/or impaired VLC-FA oxidation in peroxisomes. Higher plasma levels in VLC-ACs are surrogates of inherited peroxisomal FAO disorders such in X-linked adrenoleukodystrophy [50] and was also reported in a monogenic

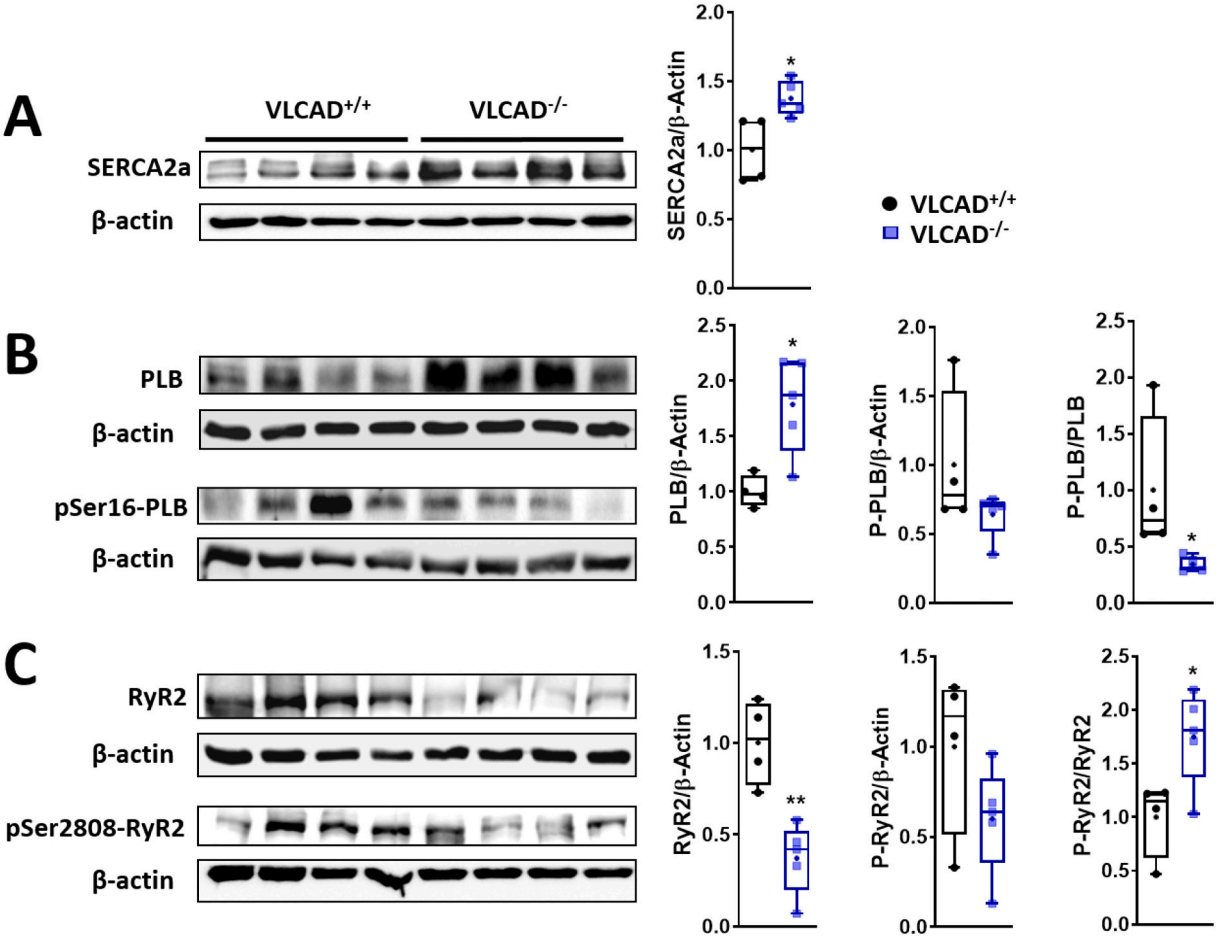

Fig. 6. Altered expression of cardiac proteins involved in calcium homeostasis in VLCAD$^{-/-}$ mice under the HFD/fasted condition.

mitochondrial disorder [32]. Although we did not find any significant changes in transcripts levels for key markers of peroxisomal β-oxidation, namely ACOX1, PTHIO, EHHADH and MFP2, further investigations of the role of peroxisomes in VLCADD appear warranted. Taken together our results do not support a role for LC-ACs accumulating intracellularly as a potential mechanism underlying the cardiac phenotype in VLCAD$^{-/-}$ mice *via* direct regulation of ion channels such as hERG [19], and calcium handling proteins such as calcium release channel, Ca(2+)-ATPase or ryanodine receptor [51–53]. The impact of VLC-ACs remains to be clarified, but it tempting to speculate that VLC-ACs may have similar effects and thus be involved in arrhythmogenesis, albeit this remains to be ascertained.

Then, we conducted additional untargeted lipidomic analysis to follow up on our previous finding of lower DHA content in GPLs in VLCAD$^{-/-}$ mouse hearts [23]. This led to a major finding of this study, which is a marked imbalance in GPLs, both PE and PC, containing C22:6 (lower) and C20:4 (higher) in VLCAD$^{-/-}$ mouse hearts *vs* controls in the HFD/fasted condition only. These changes were paralleled by those in corresponding DHA- and AA-derived metabolites from their non-enzymatic oxygenation, namely NeuroP (lower) and IsoP (higher), respectively. This finding is of particular relevance since DHA was shown to be protective against arrhythmias [28,54]. While the underlying mechanisms remain, however, to be better understood, it has been proposed that a modification of the cell membrane GPL content may affect membrane fluidity, lipid microdomain formation and signaling, which in turn would modulate the function of membrane voltage gate channels [55–58]. Moreover, DHA-derived neuroprostanes have also been shown to have anti-arrhythmogenic properties [28,29], possibly by countering cellular oxidative stress. Conversely, AA has been reported to be pro-arrhythmogenic through its enzymatically derived metabolites TXA_2 or its stable counterpart TXB_2. The latter metabolites, which were found to be higher in VLCAD$^{-/-}$ mouse heart, have been associated with arrhythmias during myocardial ischemia in an open-chest greyhound [59] or following its direct injection in the left atrium of rabbits [60]. The mechanism underlying TXA_2-induced arrhythmias is also not understood, but evidence support the involvement of the voltage-independent AA-regulated calcium (ARC) channel [61]. Consistently, the non-enzymatic oxygenated AA-derivatives, IsoP, has also been shown to be involved in the pathogenesis of arrhythmias by inactivation of cardiac Na^+ channels [62,63]. Hence, based on these considerations, our finding of a marked imbalance between cardiac DHA (lower) *vs* AA (higher) content in GPLs and their respective non-enzymatically derived oxygenated metabolites, NeuroP (lower) and IsoP (higher), suggests potential actors contributing to a pro-arrhythmogenic environment in VLCAD$^{-/-}$ mouse hearts under the HFD/fasted condition.

Regarding the molecular mechanisms that could possibly underlie GPL acyl chain remodeling in VLCAD$^{-/-}$ mouse hearts, which was exacerbated under the HFD/fasted condition, we did not find any significant changes in the gene expression of enzymes involved in PUFA synthesis. While liver is known to play an important role in PUFA and GPL metabolism [50,64], our previous findings showed that the LCFA profile, and consequently their enrichment in DHA, in GPLs in liver as well as in plasma of 7-month-old VLCAD$^{-/-}$ mice was similar to their control counterpart under both CD and HFD thereby supporting the notion that the liver export of DHA was not affected [23]. Clarification of this aspect in the future would, however, require the use of cardiac-specific VLCAD$^{-/-}$ mice. Nevertheless, our results highlighted significantly higher transcript levels of key enzymes involved in cardiac GPL

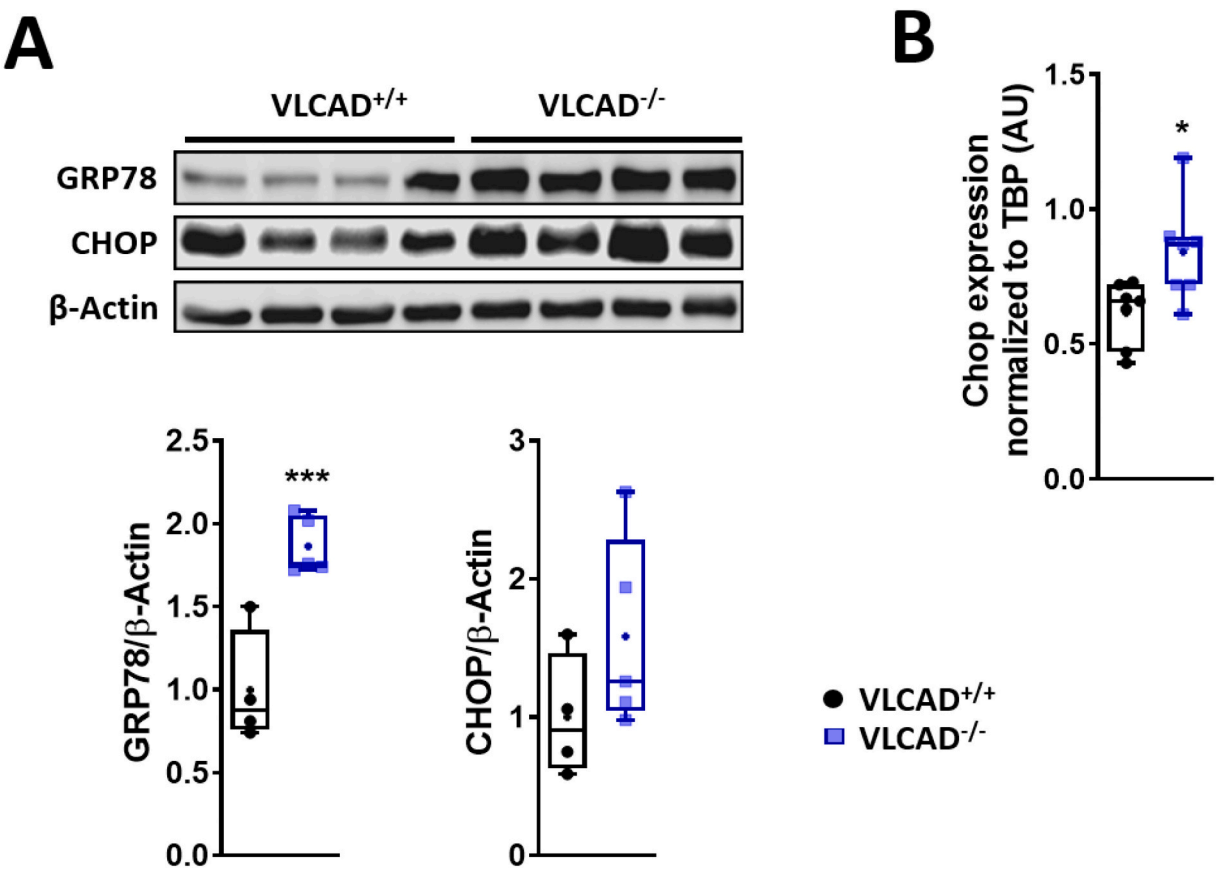

Fig. 7. Higher cardiac levels of molecular markers of endoplasmic reticulum (ER) stress in VLCAD$^{-/-}$ mice under the HFD/fasted condition.

remodeling through hydrolysis or reacylation, namely *Pla2g4* and *Lpcat2*, specifically those enzymes that are regulated by intracellular calcium [42], which was observed in both the CD/fed and HFD/fasted condition. In contrast to the CD/fed state, such changes in the HFD/fasted state were, however, not accompanied by potentially adaptive higher transcript levels for enzymes involved in the synthesis of the PUFA AA and DHA thereby suggesting one possible explanation for the specific alterations in the content of these PUFAs in GPLs in VLCAD$^{-/-}$ mouse hearts under the latter condition. Interestingly, *Pla2g4* has been reported to preferentially promote the release of AA from GPLs, generating prostanoids, which in turn induce ER stress [65], whereas *Lpcat2* reintroduce AA into the membrane GPLs [42]. Such deregulation has been described in liver from non-alcoholic fatty liver disease patients [66] and is responsible of a vicious circle referred to as "AA released-ER stress-calcium mishandling vicious cycle". Whether such cycle is also present in the heart needs to be ascertained, but likely this could promote arrhythmias following accumulation of proarrythmogenic AA derivatives, namely IsoP and TXA_2, as it was observed in VLCAD$^{-/-}$ mouse hearts under the HFD/fasted condition in this study. From a therapeutic point of view, it would be interesting to evaluate whether inhibition of AA release by *Pla2g4*, or inhibition of AA-regulated calcium channel involved in TXA2-induced arrhythmias [67], could prevent heart rhythm disorders in VLCAD$^{-/-}$ mice.

Beyond suggesting a potential role of changes in cardiac gene expression in enzymes involved in GPL acyl chain remodeling, our findings of higher transcript levels in *Lpcat2* and *Pla2g4*, but not *Lpcat3* and *Pla2g6*, point out to a prevailing calcium deregulation, which along with disturbances of bioenergetics, was previously linked to cardiac manifestations seen in VLCADD [68]. Consistent with this notion, we reported significant changes in protein expression of enzymes involved in calcium homeostasis in the heart, namely calcium-regulated SERCA2a (higher), PLB (higher) and its phosphorylation level (lower) as well as RyR2 (lower) and its phosphorylation level (higher) in VLCAD$^{-/-}$ mice. These changes were seen predominantly under the HFD/fasted condition. In mammalians heart, the proper excitation-contraction coupling is tightly regulated by release of calcium from sarcoplasmic reticulum through the RyR during systole, and reuptake of calcium in the same amount into the sarcoplasmic reticulum by SERCA pump during diastole [69]. In VLCAD$^{-/-}$ mice heart, such alterations in expression or activation of the major protein involved in calcium handling might result in imbalance between Ca^{2+} release and reuptake, as well as Ca^{2+} leak through RyR during diastole, which could induce calcium sparks and trigger arrhythmias [70]. Of potential relevance in terms of mechanisms, F_4-NeuroP derived from DHA oxidation has been shown to exert their antiarrhythmic effect by preventing sarcoplasmic reticulum Ca^{2+} accumulation *via* inhibition of posttranslational modifications of RyR2 including carbonylation, S-nitrosylation or phosphorylation on serine 2808 [29]. Hence, it appears likely that the lower level of F_4-NeuroP and higher RyR2 phosphorylation herein reported in VLCAD$^{-/-}$ mouse heart are setting conditions for the genesis of arrhythmias. Further investigations using calcium imaging, namely through recording of Ca^{2+} transients in cardiomyocytes isolated from VLCAD$^{-/-}$ mice, would indicate the changes that may impair intracellular calcium homeostasis.

Finally, we evaluated the presence of ER stress, given that it has been linked to both perturbations in lipid homeostasis [71] and calcium handling [72,73], with the latter shown to trigger ventricular arrhythmias secondary to abnormal diastolic depolarization [74]. ER stress involves the accumulation of unfolded proteins in the ER lumen [71]. The unfolded protein response (UPR) is a complex signaling pathway intending to re-establish normal ER function [72]. Our results support the induction of ER stress in VLCAD$^{-/-}$ mouse heart in the HFD/fasted, but not the CD/fed, condition based on the higher expression of GRP78 and CHOP, two proteins currently used as markers of ER stress. GRP78 is a well-established ER chaperone protein implicated in the UPR response,

which leads to increased expression of the transcription factor CHOP [75]. It is tempting to speculate that induction of ER stress in VLCAD$^{-/-}$ mouse hearts may result from GPL remodeling as previously reported by others [66,76]. Alternatively, it may also be induced by accumulation of VLC-ACs, as observed in VLCAD$^{-/-}$ mouse hearts in this study, based on findings that ER stress can be triggered by exposition to VLC-ACs metabolic precursors, namely LC-ACs as shown in skeletal muscle model (C2C12 myotubes) [14] or to VLC-FAs as shown in fibroblasts from X-linked adrenoleukodystrophy [77]. Given that ER stress has also been shown to lead to deregulated lipid metabolism [45], one would expect that there will be a vicious circle between lipid perturbations and ER stress in VLCDA$^{-/-}$ mouse hearts, which will lead to worsening of the situation with time.

Altogether, results from this study highlighted various changes in the lipid landscape in male VLCAD$^{-/-}$ mouse hearts particularly under he HFD/fasted condition, which mimics FA overload, which is known to worsen symptoms in human VLCADD. The observed lipid changes encompass VLC-AC accumulation, GPL acyl chain remodeling with higher AA and lower DHA contents and parallel variations of their respective derivatives IsoP and NeuroP. Such lipid perturbations, which were associated with alterations in proteins involved in calcium handling and ER stress, represent potential mechanisms that could contribute to the pathogenesis of arrhythmias. Further investigations are, however, needed to assess whether the aforementioned changes in male VLCAD$^{-/-}$ mice under the HFD/fasted condition can be extended to the HFD/fed condition and in female VLCAD$^{-/-}$ mice as well as are associated with cardiac functional or electrophysiological consequences. Nevertheless, the documented changes may represent potential therapeutic targets for treatments in VLCADD in mice as well as in humans.

CRediT authorship contribution statement

BL, RG, JR, FL, MR and CDR designed the study's specific aims; BL and RG critically evaluated the literature as well as performed experiments and analyzed the data under the guidance of MR and CDR; AF, BB, CD, IRF, CO and KG performed the lipidomic analysis under the supervision of JMG, TD, JFB, MR and CDR. The manuscript was written and edited by BL, RG, MR and CDR; JMG, TD and JFB critically revised the manuscript.

Declaration of competing interest

The authors have no conflict of interest to declare.

Data availability

The raw lipidomic dataset supporting the conclusion of this article has been deposited at Metabolomics Workbench (www.metabolomicsworkbench.org). The study reference number is # ST002569 and the link is: https://doi.org/10.21228/M8ND9B. Other raw data are available upon request.

Acknowledgments

We thank Jessica Larose for the analysis of data for isoprostanes and neuroprostanes. The authors also thank Lucie Lefebvre, research center, Montreal Heart Institute, for editorial and secretarial assistance.

Funding

This work was supported by grants from the French Society for Inherited Metabolic Disease. This work was supported by the Canadian Institutes of Health Research (CIHR) grants (number 9575 to CDR) as well as the Montreal Heart Institute Foundation and benefited from infrastructure supported by the Canadian Foundation for Innovation (grant numbers 20415 and 36283 to CDR).

Appendix A. Supplementary data

Supplementary Word file containing Figs. S1-S4, related to Figs. 2, and 5-7), Supplementary Tables 1–2 (related to Methods) and Supplementary Table 3 (related to Fig. 1 and 5-7) as well as an Excel file containing Supplementary Tables 4–7 (MS data linked to Figs. 1-2 and Fig. S1) to this article can be found online at https://doi.org/10.1016/j.bbadis.2023.166843.

References

[1] A. Boneh, B.S. Andresen, N. Gregersen, et al., VLCAD deficiency: pitfalls in newborn screening and confirmation of diagnosis by mutation analysis, Mol. Genet. Metab. 88 (2006) 166–170, https://doi.org/10.1016/j.ymgme.2005.12.012.
[2] J.M. Saudubray, D. Martin, P. de Lonlay, et al., Recognition and management of fatty acid oxidation defects: a series of 107 patients, J. Inherit. Metab. Dis. 22 (1999) 488–502, https://doi.org/10.1023/a:1005556207210.
[3] D. Bonnet, D. Martin, P. De Lonlay, et al., Arrhythmias and conduction defects as presenting symptoms of fatty acid oxidation disorders in children, Circulation 100 (1999) 2248–2253, https://doi.org/10.1161/01.cir.100.22.2248.
[4] J. Baruteau, P. Sachs, P. Broué, et al., Clinical and biological features at diagnosis in mitochondrial fatty acid beta-oxidation defects: a French pediatric study of 187 patients, J. Inherit. Metab. Dis. 36 (2013) 795–803, https://doi.org/10.1007/s10545-013-9628-9.
[5] M. Evans, B.S. Andresen, J. Nation, A. Boneh, VLCAD deficiency: follow-up and outcome of patients diagnosed through newborn screening in Victoria, Mol. Genet. Metab. 118 (2016) 282–287, https://doi.org/10.1016/j.ymgme.2016.05.012.
[6] B. Merinero, P. Alcaide, E. Martin-Hernandez, et al., Four years' experience in the diagnosis of very long-chain Acyl-CoA dehydrogenase deficiency in infants detected in three Spanish newborn screening centers, JIMD Rep. 39 (2018) 63–74, https://doi.org/10.1007/8904_2017_40.
[7] D. Bouvier, C. Vianey-Saban, S. Ruet, C. Acquaviva, Development of a tandem mass spectrometry method for rapid measurement of medium- and very-long-chain Acyl-CoA dehydrogenase activity in fibroblasts, JIMD Rep. 35 (2017) 71–78, https://doi.org/10.1007/8904_2016_22.
[8] A. Smon, B. Repic Lampret, U. Groselj, M., et al., Next generation sequencing as a follow-up test in an expanded newborn screening programme, Clin. Biochem. 52 (2018) 48–55, https://doi.org/10.1016/j.clinbiochem.2017.10.016.
[9] Y.E. Landau, S.E. Waisbren, L.M. Chan, H.L. Levy, Long-term outcome of expanded newborn screening at Boston children's hospital: benefits and challenges in defining true disease, J. Inherit. Metab. Dis. 40 (2017) 209–218, https://doi.org/10.1007/s10545-016-0004-4.
[10] J.C. Bleeker, I.L. Kok, S. Ferdinandusse, et al., Impact of newborn screening for very-long-chain acyl-CoA dehydrogenase deficiency on genetic, enzymatic, and clinical outcomes, J. Inherit. Metab. Dis. 42 (2019) 414–423, https://doi.org/10.1002/jimd.12075.
[11] B. Wilcken, Fatty acid oxidation disorders: outcome and long-term prognosis, J. Inherit. Metab. Dis. 33 (2010) 501–506, https://doi.org/10.1007/s10545-009-9001-1.
[12] S.C. Van Calcar, M. Sowa, F. Rohr, et al., Nutrition management guideline for very-long chain acyl-CoA dehydrogenase deficiency (VLCAD): an evidence- and consensus-based approach, Mol. Genet. Metab. 131 (2020) 23–37, https://doi.org/10.1016/j.ymgme.2020.10.001.
[13] K.I. Alatibi, S. Tholen, Z. Wehbe, J., et al., Lipidomic and proteomic alterations induced by even and odd medium-chain fatty acids on fibroblasts of long-chain fatty acid oxidation disorders, Int. J. Mol. Sci. 29 (2021) 10556, https://doi.org/10.3390/ijms221910556.
[14] C.S. McCoin, T.A. Knotts, K.D. Ono-Moore, P.J. Oort, S.H. Adams, Long-chain acylcarnitines activate cell stress and myokine release in C2C12 myotubes: calcium-dependent and -independent effects, Am. J. Physiol. Endocrinol. Metab. 308 (2015) E990–E1000, https://doi.org/10.1152/ajpendo.00602.2014.
[15] J.M. Rutkowsky, T.A. Knotts, K.D. Ono-Moore, et al., Acylcarnitines activate proinflammatory signaling pathways, Am. J. Physiol. Endocrinol. Metab. 15 (2014) E1378–E1387, https://doi.org/10.1152/ajpendo.00656.2013.
[16] G.R. Hajer, T.W. van Haeften, F.L. Visseren, Adipose tissue dysfunction in obesity, diabetes, and vascular diseases, Eur. Heart J. 29 (2008) 2959–2971, https://doi.org/10.1093/eurheartj/ehn387.
[17] B. Lefort, E. Gouache, C. Acquaviva, et al., Pharmacological inhibition of carnitine palmitoyltransferase 1 restores mitochondrial oxidative phosphorylation in human trifunctional protein deficient fibroblast, Biochim. Biophys. Acta Mol. basis Dis. 2017 (1863) 1292–1299, https://doi.org/10.1016/j.bbadis.2017.04.005.
[18] F. Labarthe, R. Gélinas, C. Des Rosiers, Medium-chain fatty acids as metabolic therapy in cardiac disease, Cardiovasc. Drugs Ther. 22 (2008) 97–106, https://doi.org/10.1007/s10557-008-6084-0.
[19] F. Ferro, A. Ouillé, T.A. Tran, et al., Long-chain acylcarnitines regulate the hERG channel, PLoS One 7 (2012), e41686, https://doi.org/10.1371/journal.pone.0041686.
[20] K.B. Cox, D.A. Hamm, D.S. Millington, et al., Gestational, pathologic and biochemical differences between very long-chain acyl-CoA dehydrogenase deficiency and long-chain acyl-CoA dehydrogenase deficiency in the mouse, Hum. Mol. Genet. 10 (2001) 2069–2077, https://doi.org/10.1093/hmg/10.19.2069.

[21] V.J. Exil, R.L. Roberts, H. Sims, et al., Very-long-chain acyl-coenzyme A dehydrogenase deficiency in mice, Circ. Res. 93 (2003) 448–455, https://doi.org/10.1161/01.RES.0000088786.19197.E4.

[22] M. Chegary, H. Brinke, J.P. Ruiter, et al., Mitochondrial long chain fatty acid beta-oxidation in man and mouse, Biochim. Biophys. Acta 1791 (2009) 806–815, https://doi.org/10.1016/j.bbalip.2009.05.006.

[23] R. Gélinas, J. Thompson-Legault, B. Bouchard, C., et al., Prolonged QT interval and lipid alterations beyond β-oxidation in very long-chain acyl-CoA dehydrogenase null mouse hearts, Am. J. Physiol. Heart Circ. Physiol. 301 (2011) H813–H823, https://doi.org/10.1152/ajpheart.01275.2010.

[24] A.J. Bakermans, T.R. Geraedts, M. van Weeghel, et al., Fasting-induced myocardial lipid accumulation in long-chain acyl-CoA dehydrogenase knockout mice is accompanied by impaired left ventricular function, Circ. Cardiovasc. Imaging 4 (2011) 558–565, https://doi.org/10.1161/CIRCIMAGING.111.963751.

[25] S. Tucci, U. Flögel, S. Hermann, M. Sturm, M. Schäfers, U. Spiekerkoetter, Development and pathomechanisms of cardiomyopathy in very long-chain acyl-CoA dehydrogenase deficient (VLCAD(-/-)) mice, Biochim. Biophys. Acta 2014 (1842) 677–685, https://doi.org/10.1016/j.bbadis.2014.02.001.

[26] L. Calò, A. Martino, C. Tota, The anti-arrhythmic effects of n-3 PUFAs, Int. J. Cardiol. 20 (2013) S21–S27, https://doi.org/10.1016/j.ijcard.2013.06.043.

[27] D. Weisman, R. Beinart, A. Erez, N., et al., Effect of supplemented intake of omega-3 fatty acids on arrhythmias in patients with ICD: fish oil therapy may reduce ventricular arrhythmia, J. Interv. Card. Electrophysiol. 49 (2017) 255–261, https://doi.org/10.1007/s10840-017-0267-1.

[28] S. Judé, S. Bedut, S. Roger, M., et al., Peroxidation of docosahexaenoic acid is responsible for its effects on I TO and I SS in rat ventricular myocytes, Br. J. Pharmacol. 139 (2003) 816–822, https://doi.org/10.1038/sj.bjp.0705308.

[29] J. Roy, C. Oger, J. Thireau, et al., Nonenzymatic lipid mediators, neuroprostanes, exert the antiarrhythmic properties of docosahexaenoic acid, Free Radic. Biol. Med. 86 (2015) 269–278, https://doi.org/10.1016/j.freeradbiomed.2015.04.014.

[30] J. Roy, J. Fauconnier, C. Oger, et al., Non-enzymaticoxidized metabolite of DHA, 4 (RS)-4-F4t-neuroprostane protects the heart against reperfusioninjury, Free Radic. Biol. Med. 102 (2017) 229–239, https://doi.org/10.1016/j.freeradbiomed.2016.12.005.

[31] X. Geng, J.M. Galano, C. Oger, G.Y. Sun, T. Durand, J.C. Lee, Neuroprotective effects of DHA-derived peroxidation product 4(RS)-4-F4t-neuroprostane on microglia, Free Radic. Biol. Med. 185 (2022) 1–5, https://doi.org/10.1016/jj.freeradbiomed.2022.04.002.

[32] M. Ruiz, A. Cuillerier, C. Daneault, et al., Lipidomics unveils lipid dyshomeostasis and low circulating plasmalogens as biomarkers in a monogenic mitochondrial disorder, JCI Insight 25 (2019), e123231, https://doi.org/10.1172/jci.insight.123231.

[33] J. Larose, P. Julien, K. Greffard, et al., F2-isoprostanes are correlated with trans fatty acids in the plasma of pregnant women, Prostaglandins Leukot. Essent. Fat. Acids 91 (2014) 243–249, https://doi.org/10.1016/j.plefa.2014.09.010.

[34] A. Dupuy, P. Le Faouder, C. Vigor, et al., Simultaneous quantitative profiling of 20 isoprostanoids from omega-3 and omega-6 polyunsaturated fatty acids by LC-MS/MS in various biological samples, Anal. Chim. Acta 921 (2016) 46–58, https://doi.org/10.1016/j.aca.2016.03.024.

[35] A. Forest, M. Ruiz, B. Bouchard, et al., Comprehensive and reproducible untargeted lipidomic workflow using LC-QTOF validated for human plasma analysis, J. Proteome Res. 17 (2018) 3657–3670, https://doi.org/10.1021/acs.jproteome.8b00270.

[36] M. Ruiz, L. Coderre, D. Lachance, et al., MK2 deletion in mice prevents diabetes-induced perturbations in lipid metabolism and cardiac dysfunction, Diabetes. 65 (2016) 381–392, https://doi.org/10.2337/db15-0238.

[37] P. Laforêt, C. Acquaviva-Bourdain, O. Rigal, et al., Diagnostic assessment and long-term follow-up of 13 patients with Very Long-Chain Acyl-Coenzyme A dehydrogenase (VLCAD) deficiency, Neuromuscul. Disord. 19 (2009) 324–329, https://doi.org/10.1016/j.nmd.2009.02.007.

[38] K. Yamada, Y. Osawa, H. Kobayashi, Y., et al., Serum C14:1/C12:1 ratio is a useful marker for differentiating affected patients with very long-chain acyl-CoA dehydrogenase deficiency from heterozygous carriers, Mol. Genet. Metab. Rep. 5 (2019), 100535, https://doi.org/10.1016/j.ymgmr.2019.100535.

[39] T.N. Tarasenko, K. Cusmano-Ozog, P.J. McGuire, Tissue acylcarnitine status in a mouse model of mitochondrial β-oxidation deficiency during metabolic decompensation due to influenza virus infection, Mol. Genet. Metab. 125 (2018) 144–152, https://doi.org/10.1016/j.ymgme.2018.06.012.

[40] O.S. Ahmed, J.M. Galano, T. Pavlickova, et al., Moving forward with isoprostanes, neuroprostanes and phytoprostanes: where are we now? Essays Biochem. 64 (2020) 463–484, https://doi.org/10.1042/EBC20190096.

[41] F. Catella, D. Healy, J.A. Lawson, G.A. FitzGerald, 11-Dehydrothromboxane B2: a quantitative index of thromboxane A2 formation in the human circulation, Proc. Natl. Acad. Sci. U. S. A. 83 (1986) A5861–A5865, https://doi.org/10.1073/pnas.83.16.5861.

[42] E.A. Dennis, J. Cao, Y.H. Hsu, V. Magrioti, G. Kokotos, Phospholipase A2 enzymes: physical structure, biological function, disease implication, chemical inhibition, and therapeutic intervention, Chem. Rev. 111 (2011) 6130–6185, https://doi.org/10.1021/cr200085w.

[43] P. Fagone, S. Jackowski, Membrane phospholipid synthesis and endoplasmic reticulum function, J. Lipid Res. 50 (2009) S311–S316, https://doi.org/10.1194/jlr.R800049-JLR200.

[44] S. Hamilton, D. Terentyev, Proarrhythmic remodeling of calcium homeostasis in cardiac disease; implications for diabetes and obesity, Front. Physiol. 30 (2018) 1517, https://doi.org/10.3389/fphys.2018.01517.

[45] X. Han, Lipidomics for studying metabolism, Nat. Rev. Endocrinol. 12 (2016) 668–679, https://doi.org/10.1038/nrendo.2016.98.

[46] D.S. Schwarz, M.D. Blower, The endoplasmic reticulum: structure, function and response to cellular signaling, Cell. Mol. Life Sci. 73 (2016) 79–94, https://doi.org/10.1007/s00018-015-2052-6.

[47] X. Rong, C.J. Albert, C. Hong, et al., LXRs regulate ER stress and inflammation through dynamic modulation of membrane phospholipid composition, Cell Metab. 18 (2013) 685–697, https://doi.org/10.1016/j.cmet.2013.10.002.

[48] Z. Liu, Y. Zhang, S. Pan, et al., Activation of RAGE-dependent endoplasmic reticulum stress associates with exacerbated postmyocardial infarction ventricular arrhythmias in diabetes, Am. J. Physiol. Endocrinol. Metab. 320 (2021) E539–E550, https://doi.org/10.1152/ajpendo.00450.2020.

[49] M. Liu, S.C. Dudley Jr., The role of the unfolded protein response in arrhythmias, Channels (Austin) 12 (2018) 335–345, https://doi.org/10.1080/19336950.2018.1516985.

[50] M.C. van de Beek, I.M. Dijkstra, H. van Lenthe, et al., C26:0-Carnitine is a new biomarker for X-Linked Adrenoleukodystrophy in mice and man, PLoS One 11 (2016), e0154597, https://doi.org/10.1371/journal.pone.0154597.

[51] K.A. Yamada, E.M. Kanter, A. Newatia, Long-chain acylcarnitine induces Ca2+ efflux from the sarcoplasmic reticulum, J. Cardiovasc. Pharmacol. 36 (2000) 14–21, https://doi.org/10.1097/00005344-200007000-00002.

[52] R. el-Hayek, C. Valdivia, H.H. Valdivia, K. Hogan, R. Coronado, Activation of the Ca2+ release channel of skeletal muscle sarcoplasmic reticulum by palmitoyl carnitine, Biophys. J. 65 (1993) 779–789, https://doi.org/10.1016/S0006-3495(93)81101-9.

[53] E. Dumonteil, H. Barré, G. Meissner, Effects of palmitoyl carnitine and related metabolites on the avian Ca(2+)-ATPase and Ca2+ release channel, J. Physiol. 15 (1994) 29–39, https://doi.org/10.1113/jphysiol.1994.sp020275.

[54] J. Endo, M. Arita, Cardioprotective mechanism of omega-3 polyunsaturated fatty acids, J. Cardiol. 67 (2016) 22–27, https://doi.org/10.1113/jphysiol.1994.sp020275.

[55] J.Y. Le Guennec, S. Jude, P. Besson, E. Martel, P. Champeroux, Cardioprotection by omega-3 fatty acids: involvement of PKCs? Prostaglandins Leukot. Essent. Fat. Acids 82 (2010) 173–177, https://doi.org/10.1016/j.plefa.2010.02.024.

[56] S.I. Liin, M.S. Ejneby, R. Barro-Soria, et al., Polyunsaturated fatty acid analogs act antiarrhythmically on the cardiac IKs channel, Proc. Natl. Acad. Sci. U. S. A. 112 (2015) 5714–5719, https://doi.org/10.1073/pnas.1503488112.

[57] D. Mozaffarian, J.H. Wu, Omega-3 fatty acids and cardiovascular disease: effects on risk factors, molecular pathways, and clinical events, J. Am. Coll. Cardiol. 58 (2011) 2047–2067, https://doi.org/10.1016/j.jacc.2011.06.063.

[58] F. Elinder, S.I. Liin, Actions and mechanisms of polyunsaturated fatty acids on voltage-gated ion channels, Front. Physiol. 8 (2017) 43, https://doi.org/10.3389/fphys.2017.00043.

[59] S.J. Coker, J.R. Parratt, I.M. Ledingham, I.J. Zeitlin, Thromboxane and prostacyclin release from ischaemic myocardium in relation to arrhythmias, Nature. 291 (1981) 323–324, https://doi.org/10.1038/291323a0.

[60] M.J. Wacker, S.R. Best, L.M. Kosloski, et al., Thromboxane A2-induced arrhythmias in the anesthetized rabbit, Am. J. Physiol. Heart Circ. Physiol. 290 (2006) H1353–H1361, https://doi.org/10.1152/ajpheart.00930.2005.

[61] M.J. Wacker, L.M. Kosloski, W.J. Gilbert, et al., Inhibition of thromboxane A2-induced arrhythmias and intracellular calcium changes in cardiac myocytes by blockade of the inositol trisphosphate pathway, J. Pharmacol. Exp. Ther. 331 (2009) 917–924, https://doi.org/10.1124/jpet.109.157677.

[62] K. Fukuda, S.S. Davies, T. Nakajima, et al., Oxidative mediated lipid peroxidation recapitulates proarrhythmic effects on cardiac sodium channels, Circ. Res. 97 (2005) 1262–1269, https://doi.org/10.1161/01.RES.0000195844.31466.e9.

[63] P.A. Boyden, S.S. Davies, P.C. Viswanathan, V. Amarnath, J.R. Balser, L.J. Roberts, Potential role of isoketals formed via the isoprostane pathway of lipid peroxidation in ischemic arrhythmias, J. Cardiovasc. Pharmacol. 50 (2007) 480–486, https://doi.org/10.1097/FJC.0b013e31815a0564.

[64] R.P. Bazinet, S. Layé, Polyunsaturated fatty acids and their metabolites in brain function and disease, Nat. Rev. Neurosci. 15 (2014) 771–785, https://doi.org/10.1038/nrn3820.

[65] G. Ren, T. Takano, J. Papillon, A.V. Cybulsky, Cytosolic phospholipase A(2)-alpha enhances induction of endoplasmic reticulum stress, Biochim. Biophys. Acta 2010 (1803) 468–481, https://doi.org/10.1016/j.bbamcr.2010.01.020.

[66] Z. Hall, N.J. Bond, T. Ashmore, et al., Lipid zonation and phospholipid remodeling in nonalcoholic fatty liver disease, Hepatology. 65 (2017) 1165–1180, https://doi.org/10.1002/hep.28953.

[67] P. Wolkowicz, P.K. Umeda, O.F. Sharifov, et al., Inhibitors of arachidonate-regulated calcium channel signaling suppress triggered activity induced by the late sodium current, Eur. J. Pharmacol. 724 (2014) 92–101, https://doi.org/10.1016/j.ejphar.2013.12.020.

[68] C. Cecatto, A.U. Amaral, J.C. da Silva, et al., Metabolite accumulation in VLCAD deficiency markedly disrupts mitochondrial bioenergetics and Ca2+ homeostasis in the heart, FEBS J. 285 (2018) 1437–1455, https://doi.org/10.1111/febs.14419.

[69] D.M. Bers, Cardiac excitation-contraction coupling, Nature. 415 (2002) 198–205, https://doi.org/10.1038/415198a.

[70] S.E. Lehnart, X.H. Wehrens, P.J. Laitinen, et al., Sudden death in familial polymorphic ventricular tachycardia associated with calcium release channel (ryanodine receptor) leak, Circulation. 109 (2004) 3208–3214, https://doi.org/10.1161/01.CIR.0000132472.98675.EC.

[71] R. Volmer, D. Ron, Lipid-dependent regulation of the unfolded protein response, Curr. Opin. Cell Biol. 33 (2015) 67–73, https://doi.org/10.1016/j.ceb.2014.12.002.

[72] S. Fu, S.M. Watkins, G.S. Hotamisligil, The role of endoplasmic reticulum in hepatic lipid homeostasis and stress signaling, Cell Metab. 15 (2012) 623–634, https://doi.org/10.1016/j.cmet.2012.03.007.
[73] Y. Xu, Z. Zhang, V. Timofeyev, et al., The effects of intracellular Ca2+ on cardiac K + channel expression and activity: novel insights from genetically altered mice, J Physiol. Feb. 562 (2005) 745–758, https://doi.org/10.1113/jphysiol.2004.076216.
[74] A.P. Landstrom, D. Dobrev, X.H.T. Wehrens, Calcium signaling and cardiac arrhythmias, Circ. Res. 120 (2017) 1969–1993, https://doi.org/10.1161/CIRCRESAHA.117.310083.
[75] M. Ni, Y. Zhang, A.S. Lee, Beyond the endoplasmic reticulum: atypical GRP78 in cell viability, signalling and therapeutic targeting, Biochem. J. 434 (2011) 181–188, https://doi.org/10.1042/BJ20101569.
[76] S. Fu, L. Yang, P. Li, et al., Aberrant lipid metabolism disrupts calcium homeostasis causing liver endoplasmic reticulum stress in obesity, Nature. 473 (2011) 528–531, https://doi.org/10.1038/nature09968.
[77] M.C. van de Beek, R. Ofman, I. Dijkstra, et al., Lipid-induced endoplasmic reticulum stress in X-linked adrenoleukodystrophy, Biochim. Biophys. Acta 2017 (1863) 2255–2265, https://doi.org/10.1016/j.bbadis.2017.06.003.